Landscape Ecol (2010) 25:889–902
DOI 10.1007/s10980-010-9466-1

RESEARCH ARTICLE

Multiscale comparison of spatial patterns using two-dimensional cross-spectral analysis: application to a semi-arid (gapped) landscape

Nicolas Barbier · Pierre Couteron · Olivier Planchon · Abdoulaye Diouf

Received: 1 July 2009 / Accepted: 24 February 2010 / Published online: 21 March 2010

Abstract Spectral analysis allows the characterization of temporal (1D) or spatial (2D) patterns in terms of their scale (frequency) distribution. Cross-spectral analysis can also be used to conduct independent correlation analyses at different scales between two variables, even in the presence of a complex superposition of structures, such as structures that are shifted, have different scales or have different levels of anisotropy. These well-grounded approaches have rarely been applied to two-dimensional ecological datasets. In this contribution, we illustrate the potential of the method. We start by providing a basic methodological introduction, and we clarify some technical points concerning the computation of two-dimensional coherency and phase spectra and associated confidence intervals. First, we illustrate the method using a simple theoretical model. Next, we present a real world application: the case of patterned (gapped) vegetation in SW Niger. In this example, we investigate the functional relationships between topography and the spatial distribution of two shrub species, *Combretum micranthum* G. Don. and *Guiera senegalensis* J.F. Gmel. We show that both the global vegetation pattern and the distribution of *C. micranthum* are independent at all analyzable scales (i.e., from 10 to 50 m) from possible relief-induced determinisms. Additionally, the two dominant shrub species form distinct patches, thus suggesting separate niches.

Nomenclature Hutchinson et al. (1954).

Electronic supplementary material The online version of this article (doi:10.1007/s10980-010-9466-1) contains supplementary material, which is available to authorized users.

N. Barbier (✉)
FNRS. Université Libre de Bruxelles, Laboratoire de Complexité et Dynamique des Systèmes Tropicaux, CP 169, 1050 Bruxelles, Belgium
e-mail: nbarbier@ulb.ac.be

N. Barbier · P. Couteron
IRD, UMR botAnique et bioinforMatique de l'Architecture des Plantes (AMAP), Boulevard de la Lironde, TA A-51/PS2, 34398 Montpellier Cedex 05, France

O. Planchon
IRD – Institut de recherche pour le développement, Kasetsart University, Po Box 1025, Bangkok 10903, Thailand

A. Diouf
Laboratoire d'Ecologie du Paysage et des Systèmes de production végétale, Université Libre de Bruxelles, 50 Av. F. Roosevelt CP 169, 1050 Bruxelles, Belgium

A. Diouf
Laboratoire GARBA Mounkaila de Biologie, Université ABDOU Moumouni, BP: 10 662, Niamey, Niger

Keywords Map comparison · Cross-covariance · Two-dimensional Fourier transform · Spatial ecology · Self-organization · Periodic vegetation patterns · Tiger bush · Niger

Introduction

When investigating correlations between spatial variables in ecology, one is generally confronted with two well-known issues: (i) the nature of the relationship between variables varies with scale (Wiens 1989; Levin 1992; Schneider 2001) and (ii) each variable is more or less spatially autocorrelated (Legendre 1993). If evidencing correlation remains a key step in the identification of processes from patterns (McIntire and Fajardo 2009), a broad set of ecological examples has been presented in the literature that show how the scale of investigation may influence the nature of inter-variable dependence. In landscape ecology, it is often found that processes influencing the distribution or abundance of organisms within patches are different than those acting between patches (Forman and Godron 1986). However, defining patch boundaries may be difficult. For instance, the biological variable of interest may vary continuously through space as is often the case in arid and semi-arid areas (Puech 1994), instead of showing sharp ecotones. Furthermore, analyzing the relationship between two variables across a set of patches is not straightforward because values obtained in distinct patches cannot a priori be assumed to be independent due to the overall spatial configuration of the patches. It is then necessary to quantify the correlation structure of the variables of interest in a spatially explicit manner, for instance via auto- (cross-) correlation methods or related geostatistical functions (Cressie 1993; Wackernagel 1995).

Analyses of spatial correlations using standard tools of spatial ecology are in some instances very difficult, as is the case when there are spatial shifts (lags) between variables, or when structures at different scales or with different levels of anisotropy are superposed. Additionally, a well-organized spatial structure of a biological variable might not reflect the blueprint of an external driver. For instance, this can occur when self-organized patterns of biomass or organisms emerge from local, inter-individual interactions in fairly homogeneous environmental conditions. These self-organized structures are known to take very peculiar forms at a much larger scale than the size of the constitutive individuals, such as a spatially periodic distribution of the vegetation biomass or a power law distribution of patch sizes (Lefever and Lejeune 1997; Rohani et al. 1997; Pascual and Guichard 2005; Solé and Bascompte 2006; Rietkerk and van de Koppel 2008). To find evidence of self-organization in nature, it is necessary to establish the independence of the biological structure from potential physical drivers across a relevant range of scales. In their seminal paper, Platt and Denman (1975) demonstrated the potential of cross-spectral and spectral analysis analysis in the face of the very likely existence of endogenous structuring processes in ecosystems. Because of data and computational limitations in the 1970s, they focused on one-dimensional problems. Yet the need for bi-dimensional tools has increased with the rapidly increasing availability of remote sensing products and other georeferenced information sources.

Spectral estimates of a signal are closely related to the autocovariance function (Ripley 1981; Diggle 1989; Wackernagel 1995), as the periodogram is the Fourier transform of the latter. Fourier (cross-) spectra, however, possess specific properties and are widely recognized as a basic tool in many fields of science, even if mostly in one-dimensional contexts. Bi-dimensional applications are ubiquitous in the pattern recognition sciences (Chen et al. 1999; Tang and Stewart 2000) and are used for industrial quality control, medical image analysis, character recognition in document processing and for data compression. Rayner (1971) presented interesting bi-dimensional applications in geography. However, applications to spatial ecology remain very limited, despite the efficiency of spectral analysis for characterizing and comparing patterns from either gridded or mapped-point data (Ford 1976; Renshaw and Ford 1983, 1984; Mugglestone and Renshaw 1998; Couteron 2002; Renshaw 2002; Couteron et al. 2005, 2006; Barbier et al. 2006; Proisy et al. 2007).

The principle of spectral analysis is to partition the variance (also termed power by reference to signal

processing) of a signal into a finite set of harmonic frequencies. In other words, the structure present in the series of observations is re-expressed as the amount of variability accounted for by different scales (or frequencies, i.e. the number of repetitions) over the sampling window. The investigated signal may be uni- or multi-dimensional, continuous or discrete. In the latter case, contiguous observations (grids) can be analyzed, as well as marked point maps (Renshaw 2002). A substantial amount of non-stationarity in the data can also be accounted for (Priestley 1981; Fuentes 2002) inter alia using windowed (local) approaches related to the short-term Fourier transform. Pairs of signals can be compared through cross-spectral analysis to identify frequencies dominant in both signals, as well as possible shifts (phase lags/leads) among them. However, the use of cross-spectral analyses has remained very limited in ecology (but see Couteron 2001), and its potential for characterizing or disentangling patterns of spatial dependence at multiple scales has remained widely ignored.

Our aim here is to illustrate this potential when looking for scale-specific co-variation between pairs of ecological variables. Although the method also applies to the comparison of point patterns (Mugglestone and Renshaw 1996a, Couteron 2001), we will use gridded (two-dimensional) datasets. We use simulated examples and a field case from our research on vegetation patterning in SW Niger. In the latter case, regular vegetation patterns made of gaps in a shrubland matrix are thought to have emerged at the landscape scale from plant-plant interactions in the absence of notable preexisting substratum heterogeneities (Lefever and Lejeune 1997; HilleRisLambers et al. 2001; von Hardenberg et al. 2001; Barbier et al. 2008). However, relationships between species and the global pattern, as well as possible external causalities, need to be investigated. In particular, it has been hypothesized in the theoretical literature that the gapped patterns may be due to the existence of a micro-topography that induces water run-off from bare areas to thickets (Klausmeier 1999). We will show how these issues, which amount to comparing pairs of mapped variables, can efficiently be addressed using the cross-spectral methodology.

Methods

Analysis of spatial co-variations

The fundamental principle of the Fourier transform is to decompose a signal in terms of frequencies (i.e., the inverse of the wavelength or scale of the pattern) using a series of convolutions with sine and cosine functions of varying harmonic frequencies. While all the original information is preserved, this transformation from geographic space to frequency space is a very efficient way to characterize and compare the structure of periodic and even non-periodic signals. Consider two discrete signals made of contiguous sampled data forming rectangular grids of size (m,n), V_{ij} and W_{ij} ($i = 1,\ldots,m, j = 1,\ldots,n$), centered by their means. We wish to compute their Fourier transform for a discrete set of integer (harmonic) frequencies, $p = 1, 2, \ldots, m/2$ and $q = 1, 2, \ldots, n/2$, taken along the two Cartesian axes. We first compute the Fourier coefficients, $a(p,q)$ and $b(p,q)$, for each combination of the frequencies:

$$a_V(p,q) = (nm)^{-1} \sum_i^m \sum_j^n V_{i,j} \cos[2\pi(pi/m + qj/n)]$$

and

$$b_V(p,q) = (nm)^{-1} \sum_i^m \sum_j^n V_{i,j} \sin[2\pi(pi/m + qj/n)].$$

We do the same calculations for the other grid to obtain homologous coefficients $a_W(p,q)$ and $b_W(p,q)$. Note that in practice, the Fourier coefficients can be obtained using the efficient FFT (Fast Fourier Transform) algorithm, available in many programming environments (e.g., C, R, Matlab and IDL). The value of the discrete Fourier transform of the signal at frequencies (p,q) is simply given by the complex sum of the coefficients:

$$F_V(p,q) = a_V(p,q) + ib_V(p,q) \text{ and}$$
$$F_W(p,q) = a_W(p,q) + ib_W(p,q)$$

where i is the imaginary number. The highest frequency, ($p = n/2$, $q = m/2$), that can be discriminated along each Cartesian direction is called the

Nyquist frequency, and it is conditioned by the discrete sampling rate of the signal. In other words, details smaller than two sampling cells cannot be discriminated.

The periodogram (or sample spectrum) is given by the squared amplitude of the complex Fourier transform, that is:

$$I_V(p,q) = (nm)^{-1}(a_V(p,q)^2 + b_V(p,q)^2) \text{ and}$$
$$I_W(p,q) = (nm)^{-1}(a_W(p,q)^2 + b_W(p,q)^2)$$

Periodogram values express the apportioning of the signal variance (or power), σ^2, into integer frequency bins, (p, q), which implies that:

$$(mn)^{-1}\sum_p \sum_q I(p,q) = \sigma^2.$$

One problem in spectral analysis is controlling for the variance of the periodogram, $I(p,q)$, which is necessary to obtain accurate statistical estimates of the 'true' value from a sample of finite size. Indeed, the variance of each entry in a periodogram does not tend to zero as n increases (Diggle 1989). Whatever the length of the signal sampled, $I(p,q)$ is indeed computed from a unique observation, i.e., the portion of variance expressed by frequencies (p,q) in a given signal. However, the periodogram is a discrete approximation of a theoretically continuous function, i.e., the variance spectrum, so that the variance can be controlled by smoothing the periodogram over contiguous frequencies (Jenkins and Watts 1968; Bloomfield 1976; Diggle 1989). In all analyses performed here, we applied a moving average of order $o = 1$ (i.e., a square window of sides $2o + 1 = 3$) to the bi-dimensional periodogram and cross-periodogram (Fig. 1).

Fourier-based analogues of cross-covariance functions can also be computed on the basis of the cross-periodogram, I_{VW}:

$$\begin{aligned} I_{VW}(p,q) =& (nm)^{-1}(a_V(p,q)a_W(p,q) \\ &+ b_V(p,q)b_W(p,q)) \\ &- i(nm)^{-1}(b_V(p,q)a_W(p,q) \\ &+ a_V(p,q)b_W(p,q)). \end{aligned}$$

Contrary to the periodogram, the cross-periodogram is complex, with a real part $c_{vw}(p,q)$ and an imaginary part $d_{vw}(p,q)$,

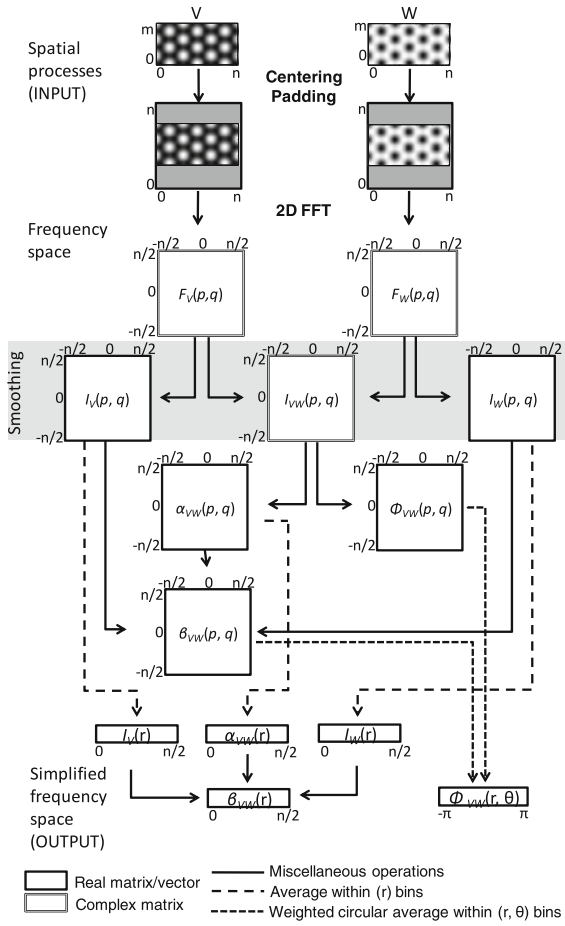

Fig. 1 Methodological flowchart

$$I_{VW}(p,q) = c_{VW}(p,q) + id_{VW}(p,q)$$

or, equivalently, an amplitude:

$\alpha_{VW}(p,q) = \sqrt{c_{VW}(p,q)^2 + d_{VW}(p,q)^2}$, called the cross-amplitude spectrum, and a phase,

$\Phi_{VW}(p,q) = \tan^{-1}[d_{VW}(p,q)/c_{VW}(p,q)]$, called the phase spectrum.

The terms $\alpha_{VW}(p,q)$ and $\Phi_{VW}(p,q)$ express the covariance and the phase shift, respectively, between structures of identical frequencies existing in the two signals. For interpretation, it is convenient to compute the coherency spectrum:

$$\beta_{VW}(p,q) = \alpha_{VW}(p,q)/\sqrt{I_V(p,q)I_W(p,q)}$$
$$\text{with } \beta_{VW}(p,q) \in [0,1],$$

which is the normalization of $\alpha_{VW}(p,q)$. The coherency spectrum expresses the correlation between the

frequency components of the two mapped variables, and it can be used to characterize how the correlation between the two changes with scale and orientation. Coherency values are interpreted in a similar way to the classical Pearson's correlation coefficient but in absolute values, where the sign of the correlation is expressed by the phase spectrum. When the coherency is high, the phase spectrum provides additional information for investigating spatially shifted inter-map dependence. A positive linear relationship corresponds to a null phase shift and a negative linear relationship to a phase shift of π, but all phase shifts between $-\pi$ and π are also possible.

Polar representation and simplification

The different spectra discussed above may be represented as square matrices in which frequencies along the two Cartesian directions (p, q) form the rows and columns, with the zero frequency usually appearing in the middle (Fig. 1). Indeed, frequencies can take negative values, where the sign indicates the direction of travel of the wave. Contrary to the phase spectrum, the periodogram and coherency spectrum are symmetric about the origin, as they only contain information on the amplitude of the waves. Interpretability of the spectra can be enhanced by using a polar representation of the frequency space, using the wavenumber:

$$r = \sqrt{p^2 + q^2}$$

and orientation,

$$\theta = \tan^{-1}\left(\frac{p}{q}\right)$$

as a basis.

In other words, each cell of the matrix contains the spectral or cross-spectral information related to a given scale (i.e., frequency) and direction. The Fourier transform is an exhaustive representation of the original signal, where the original signal can be reconstructed by the inverse transform. The spectral and cross-spectral functions, which are simplified versions, are still very rich in information, and therefore of somewhat limited interpretability. It is often desirable to further simplify this information to focus on the particular feature of interest. For instance, if one is only interested in the frequency information (i.e., only the scale at which a process occurs), the spectra can be simplified by averaging values within frequency bins r_i over all orientations to obtain an azimuthally averaged version, denoted r-spectrum (Mugglestone and Renshaw 1998). This simplification is justified if the pattern of interest is fairly isotropous, or more generally, if one does not wish to investigate the variation in pattern properties for different orientations. The computation of the r-spectrum requires frequency units (wavenumbers) to be identical in both Cartesian directions, i.e., the signal must be sampled using a square window. If a signal sampled in a rectangular window is to be analyzed, a solution is to add rows or columns of average values (or zeros for the centered signal) at the edges or the grid's narrowest dimension, prior to performing the Fourier transform (Fig. 1). This operation is referred to as padding. For the coherency spectrum, it is not advisable to compute the r-spectrum directly from the bi-dimensional coherency spectrum because ratios should not be averaged (M. Mugglestone, personal communication). A better procedure is, therefore, to divide the r-spectrum of the cross-amplitude spectrum, $\alpha_{VW}(r)$, by the r-spectra of the two smoothed periodograms (i.e., $I_V(r)$ and $I_W(r)$) (Fig. 1):

$$\beta_{VW}(r) = \alpha_{VW}(r)/\sqrt{I_V(r)I_W(r)}.$$

Regarding the phase spectrum, all frequency/orientation bins are attributed a phase value, which can be confusing if there is low coherency between the structures. The resulting diagram can be very complex, as the values for adjacent positions in the spectrum then take random values. Other difficulties lie in the circular nature of phase data (for a given entry), for which shifts of $-\pi$ and π are equivalent. Also, phase information is not symmetric about the origin of the 2D spectrum. For example, if wave A lags wave B by $\pi/3$ in one direction, it leads it by $2\pi/3$ in the opposite direction. These properties necessitate a slightly more complex simplification procedure than for the coherency spectrum. It is indeed impossible to simply average across directions to produce the phase analogue of the r-spectrum. First of all, as phase information is only meaningful for frequencies at which patterns are coherent, we only consider phase data for specific frequency ranges that

correspond to peaks in the coherency r-spectrum. Within these ranges, the phase values are to be separately averaged within orientation bins (to account for the symmetry issue). To account for the circularity of the phase data, circular averaging (Fisher 1993) is required. We further weight the phase values within each frequency/orientation bin by the corresponding value of the coherency spectrum, following a weighted circular averaging method (Fig. 1):

$$C_{bin} = \sum_{i \in bin} \beta_i \cos \Phi_i \text{ and } S_{bin} = \sum_{i \in bin} \beta_i \sin \Phi_i,$$

where the i's belong to a bin that is a subset (r, θ) of the frequency space. The weighted mean phase in the bin is then given by:

$$\bar{\Phi}_{bin} = \tan^{-1}\left(\frac{S_{bin}}{C_{bin}}\right).$$

In the above procedure, the phase entries within the bin are equivalent to vectors of angle Φ_i and module β_i. The mean phase in the bin is then the angle of the sum of vectors. Therefore, the resulting simplified phase spectrum provides information regarding the phase shift between the two maps in each direction for a specific scale range over which the patterns are coherent. The result is a plot for which phase information is given only for the frequencies and orientations in which the two maps are highly coherent.

Information regarding the computation of confidence intervals for cross-spectral estimates can be found in Appendix.

Simulated examples

We use simple simulated maps to illustrate the potential of the cross-spectral approach for interpreting two-dimensional gridded data. Two different rectangular images (50 × 100 pixels), to which we shall refer as examples 1 and 2, were created by superimposing independent components featuring distinct spatial structures (Fig. 2). To facilitate comparison with real-world images, we used an arbitrary scaling convention of 1 m/pixel.

Two fractal structures were first produced (fractional Brownian motion, Hurst exponent = 0.5, see Appendix of Keitt 2000) to represent realistic 'neutral' landscapes (Fig. 2a,e), in which the amplitude of heterogeneities depends on their scale (where the log amplitude is linearly proportional to the log frequency). A second component was then superimposed for each example: a combination of three sine functions oriented at 60° angles from each other with a spatial frequency of 6 cycles/hm (i.e., 6 periods repeated along the image length of 100 m, or a wavelength of 16.7 m). In example 1, all sine components had a phase of zero, and the resulting hexagonal pattern comprised white islands in a black matrix (hexagons 0, Fig. 2b). In example 2, a phase shift of π was added to each sine function, which produced black islands (hexagons π, Fig. 2f). A third component was then added to each example in the form of either sine (Fig. 2c) or cosine (Fig. 2g) functions that were oriented at 45° (trigonometric convention) with a frequency of 15 cycles/hm. In the combined structures (Fig. 2d,h),

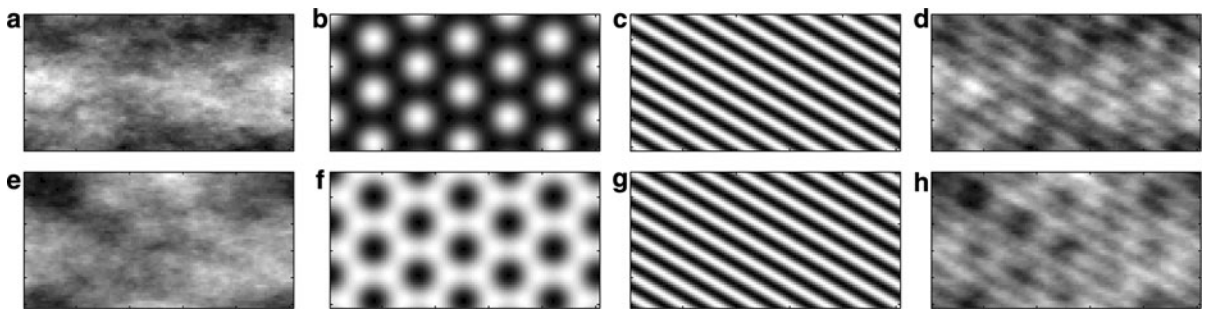

Fig. 2 Building multiscale simulated structures. **a**, **e** Colored red noise obtained using fractal Brownian motion (fBm); $\sigma \geq 3$. **b**, **f** Patterns produced using three periodic components with a frequency of 6 cycles/hm (i.e., 1 hm = 100 m, the arbitrary length of the simulated windows), and oriented at 60° angles from each other. In (**b**), the three components are in phase, producing a hexagonal lattice of white gaps. In (**f**), the three components are shifted by π. The hexagonal lattice features black islands, which is the reverse of pattern (**b**); $\sigma = 1.2$. **c**, **g** Sine (**c**) and cosine (**g**) functions oriented at 45°; $\sigma = 0.7$. **d**, **h** Sum of the three components (red noise + hexagons + bands). Signal to noise ratio equals ca. 1/3

the periodic components (hexagons and bands) were quite concealed by the fractal noise, as the signal-to-noise ratio of each periodic pattern of interest was 1/3.

Field study

As a study case, we applied the cross-spectral approach to vegetation and topography data collected in typical gapped vegetation in SW Niger (UTM 31 N 1368540 Northing, 435140 Easting) that was located on an iron-capped plateau included in the 'W' regional park (MAB-UNESCO Biosphere Reserve). The vegetation pattern was clearly dominated by a periodic structure with a spatial frequency of 2 cycles/hm, i.e., a wavelength of 50 m, a patterning scale characterizing periodic vegetations over an area of at least 3000 km^2 near the site (Barbier et al. 2006). Dominant species were tall shrubs mainly of the species *Combretum micranthum* G. Don. Shallow (30–50 cm) sandy-clay soils with high gravel content overlaid a moderately hardened iron pan (Barbier et al. 2008). Both vegetation and substratum properties were typical of the spatially regular vegetation patterns found on lateritic plateaus in Southwestern Niger.

One representative area (120 m × 70 m) was delimited (Fig. 3a), which comprised at least one wavelength (50 m) of the gapped pattern in all directions. To avoid edge effects (in particular for the TMI, see below), only a subset (105 m × 55 m) of this area was used in the spectral analyses. The plot was first subdivided into a 10 m grid, where the nodes of the grid were marked in the field using painted metallic stakes. Distances and vertical and horizontal angles between adjacent nodes were surveyed using a total station, or tacheometer, consisting of an optical theodolite (Metland MTXO^{TM}) to which was adapted a laser telemeter (Leica Disto^{TM}). Global 3D Cartesian coordinates were estimated through nonparametric least squares adjustment (Anderson and Mikhail 1998). According to the residual errors after adjustment, the horizontal angles, vertical angles, and distances were assessed with a standard error of 0.16 grad, 0.064 grad and 14 mm, respectively. The precision of the calculated location of the mesh points was estimated using Monte Carlo analysis. Based on this analysis, the standard deviation of the point locations was 18 mm horizontally and 8 mm vertically. Supplementary elevation points were collected between the nodes of the primary grid every five meters, which

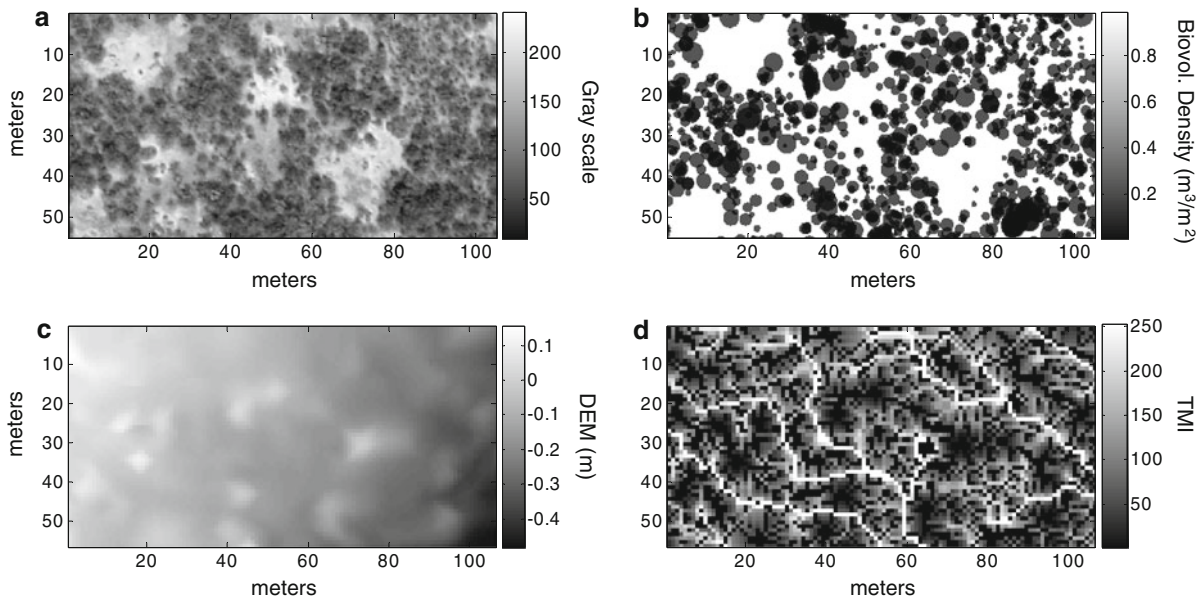

Fig. 3 Vegetation and topographical features in the study area. **a** Vertical low altitude aerial picture (bare soil appears in white and dense vegetation in dark gray). **b** Mapped biovolume density (dense vegetation appears in black). **c** Digital elevation model interpolated between the nodes on a five-meter grid. **d** Topographic Moisture Index computed from the DEM

determined the actual resolution of the resulting digital elevation model (DEM). An interpolated DEM plot is shown in Fig. 3c. This interpolation was used to aid visual interpretation. However, scales finer than 10 m (corresponding to the actual Nyquist frequency of the data) were not interpreted in the subsequent analyses involving topography layers.

To study the dependence between the vegetation pattern and topography, the relative elevation is not directly relevant. Rather, we should look at the effect of elevation on the surface redistribution (run-off) of water during rainstorms. Therefore, we derived a topographic moisture index (TMI, Fig. 3d) for each spatial cell. The TMI was equal to $\ln(\alpha/\tan(\beta))$, where α is the upslope contributing area computed following the multiple direction flow algorithm of Quinn et al. (1995), and β is the local slope. This index is a good approximation of the propensity of a cell to receive and capture run-off and considers solely local and global topography (Quinn et al. 1995; Sorensen et al. 2005). The issue of edge effects was addressed by performing the spectral analyses on a subset of the initial area (see above).

All shrubs present in the study area with a height above 1.5 m ($n = 1082$) were mapped using the tacheometer. Their heights and two perpendicular diameters were measured, and a biovolume index was computed as the height multiplied by the ellipsoidal approximation of crown area (Couteron and Kokou 1997). A map of cumulated biovolume density (Fig. 3b) was then computed. A very high-resolution (16 cm/pixel) vertical digital photograph was taken during a low altitude (150 m) flight over the study site. The photograph was georeferenced to the nearest half meter using previously set painted landmarks. The portion of the photograph corresponding to the site is shown (Fig. 3a) after conversion to gray-scale levels.

Results

Simulated example

In simple scatter plots of the pixel values from the simulated images (Fig. 2), it appears that the two fractal Brownian motion (fBm) structures do not show any clear pattern of correlation (Fig. 4a). The two hexagonal structures present a perfect negative linear correlation, with one being the exact opposite pattern of the other (Fig. 4b). The sine and cosine functions are linearly uncorrelated (they are orthogonal by definition), despite their identical scale and orientation. Interestingly, for a sufficient amplitude of the red noise (signal-to-noise ratio equals ca. 1/3 in our example), the combined structures are not correlated with each other ($R^2 = 0.04$).

The two-dimensional cross-correlogram (Fig. 5a), a familiar tool to ecologists, presents the spatial correlation between the two compared structures in a two-dimensional context, but it is very difficult to simplify to a few characteristic traits. The correlation rises and falls with distance lags. It merely reproduces the shifted small wavelength sine waves on the one hand, and the large wavelength spotted/gapped structures on the other, with limited opportunity for extracting the main features of the superimposed patterns. The 2D coherency spectrum, on the contrary, directly leads to quantifying the main properties of the covariation in the patterns. We first recall that the coherency information is symmetric about the origin, and therefore we can focus on half of the spectrum (e.g., the upper half), which displays two salient features: (i) a patch of high coherency for frequencies ($\boldsymbol{r}$) of about 15 cycles/hm with an approximate θ angle of 45°, and (ii) a ring of high coherency values for $\boldsymbol{r}$ = ca. 6 cycles/hm. More information is available in the phase spectrum, which

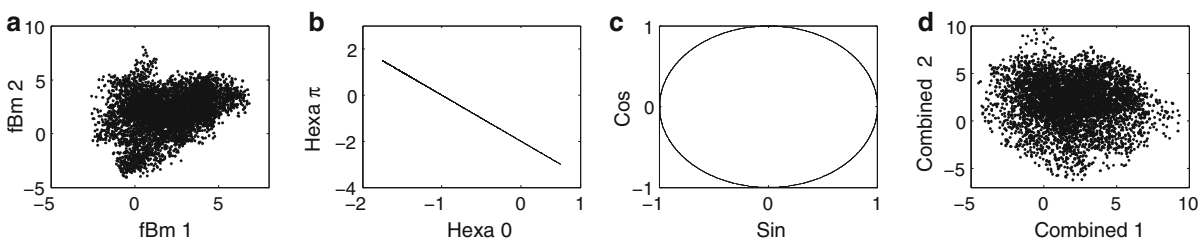

Fig. 4 Scatter plots of pixel values for the two simulated examples. **a** Comparison of the colored noise components. **b** Comparison of the hexagonal patterns. **c** Comparison of the banded patterns. **d** Comparison of the combined signals

is not symmetric about the origin (Fig. 5c). The cross-phase space might seem difficult to interpret because of large shifts in value due to the circular nature of the information (a discontinuity in angle values between $-\pi$ and π) and because areas where coherency is low tend to take random phase values. But if we only focus on the zones that had a high coherency in the coherency plot (Fig. 5b), we can easily recover that (i) the two periodic functions that are coherent around 15 cycles are shifted by $\pi/2$ (or $-\pi/2$), while the structures of lower frequency are shifted by π (or $-\pi$).

After simplification to one-dimensional plots, the same information is available in a very synthetic form (Fig. 6). The coherency r-spectrum shows two well-defined and significant peaks. The first peak, at a frequency of 6 cycles/hm, corresponds to the two hexagonal structures, while the second peak, at 15 cycles/hm, is the result of the two nearly identically banded patterns. We extracted the phase information (Fig. 6b) for areas of the frequency space for which coherency between the two signals was higher than 0.5 (that is, the ring-shaped areas corresponding to the coherency peaks at 6 and 15 cycles/hm in Figs. 5b and 6a) by computing the weighted (by the coherency values) circular mean of the phase. Using circular statistics avoids the problem of angular discontinuity. We see that the phase shift between the two signals at the frequency of the hexagonal patterns (about 6 cycles/hm, plotted in light gray) has a value of π (or $-\pi$) in the directions of the initial periodic functions (at 60° of intervals). On the other hand, the phase shift at the higher frequency of the bands (15 cycles/hm, plotted in dark gray) has a different value of $\pi/2$, towards the direction of the oblique pattern (45° or $\pi/4$).

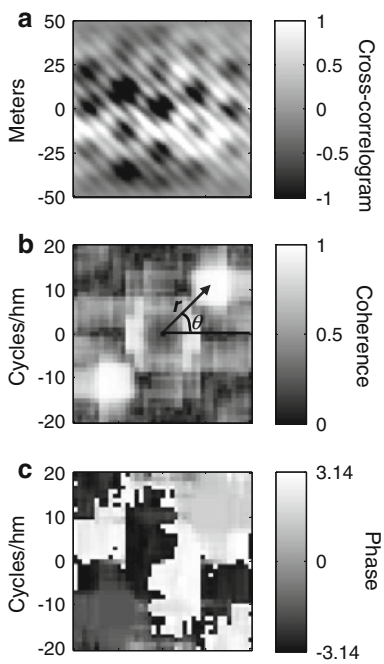

Fig. 5 Two-dimensional characterization of spatial structure. **a** Cross-correlogram (lag distances in meters). **b** Coherency spectrum, $\beta_{VW}(p,q)$. **c** Phase spectrum, $\Phi_{VW}(p,q)$

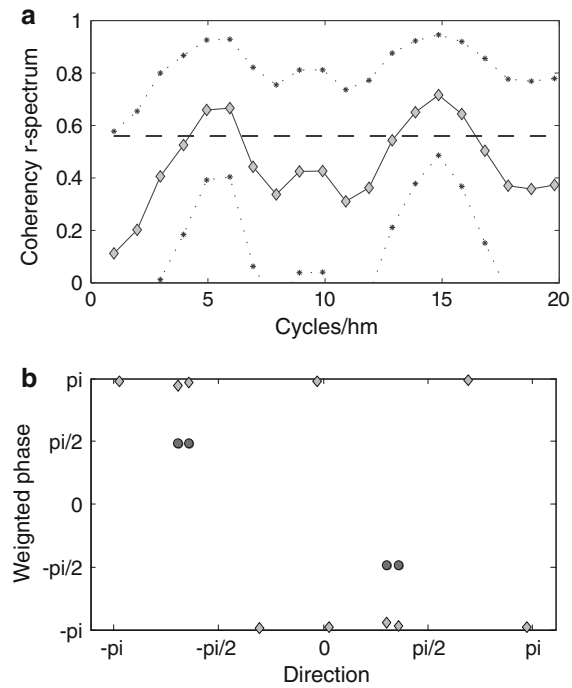

Fig. 6 Cross-spectral analysis of the combined simulated images. **a** Coherency r-spectrum. Diamonds: smoothed estimator. Dots: confidence intervals (CI) indicating two standard deviations (95%) on each side of the smoothed estimator. Dashes: confidence threshold indicating the 95% test for difference from null coherency. Note the two significant peaks around 6 and 15 cycles/hm. **b** Coherency-weighted average value of the phase for the frequencies and directions in which coherency is maximized. Light diamonds: value of the phase at the first coherency peak (6 cycles/hm). Dark circles: value of the phase at the second coherency peak (15 cycles/hm)

Field study

As a verification of the consistency of both data and methods, we first studied the relationship between the

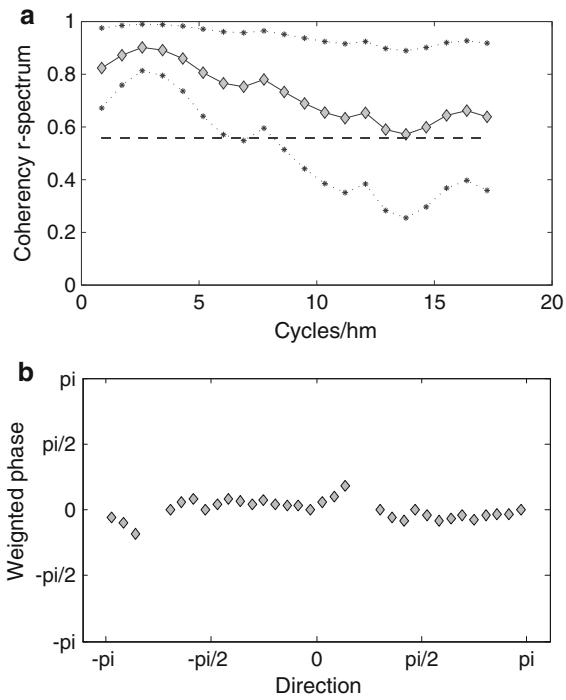

Fig. 7 Cross-spectral comparison between the biovolume density map and the vertical aerial view in gray scale. **a** Coherency r-spectrum. Diamonds: smoothed estimator. Dots: confidence intervals (CI) indicating two standard deviations (95%) on each side of the smoothed estimator. Dashes: confidence interval indicating the 95% test for difference from null coherency. **b** Coherency-weighted average value of the phase for the frequencies and directions in which coherency is maximized (approximately 2 cycles/hm)

biovolume density maps (i.e., the vegetation as mapped in the field) and the gray-scale values of the aerial view (data shown in Fig. 3a,b). The coherency r-spectrum shows values above 0.6 for all considered frequencies and up to 0.9 for frequencies around 2 cycles/hm (Fig. 7a), i.e., those corresponding to the wavelength of the periodic pattern (i.e., 50 m). Coherency values are significantly different from zero across the whole spectrum. The phase spectrum, on the other hand, consistently presents a phase shift close to zero, which indicates a good alignment between the two maps (Fig. 7b). Therefore, the coherency spectrum confirms that a strong positive correlation exists between the two representations at all analyzable spatial scales. Note that the lower correlation for large frequencies mainly comes from the fact that shrubs below 1.5 m height and the grass layer were not taken into consideration in the biovolume survey, while they clearly influenced the fine-grained details of the aerial view. This fact does not impair our analysis, but on the contrary, underscores the importance of a scale-specific approach. Indeed, the global (Pearson's) correlation coefficient between the two processes, although very significant (Monte Carlo test with random toroidal translations, $P < 0.001$), is only 0.51. Nearly identical results were obtained when considering the biomass density map of *Combretum micranthum*, the dominant shrub species, instead of the total biovolume.

When applied to the study of the relationship between vegetation density and micro-topography (DEM, Fig. 3c), the cross-spectral analysis shows a clear independence (i.e., coherency values not significantly different from zero) between the two variables (result not shown). In other words, the vegetation cover at all scales is independent from topography. The same result was found when we considered the relationship between vegetation cover and the topographic moisture index (TMI, Fig. 3d), which takes into account both the upslope contributing area and the local slope for each point (Fig. 8). Coherency values were near 0.4 throughout the spectrum and not significantly different from zero according to the confidence boundaries, even at the scale of the periodic vegetation pattern (2 cycles/hm). Here again, *C. micranthum*, the dominant species, behaved in the same manner as the total vegetation cover.

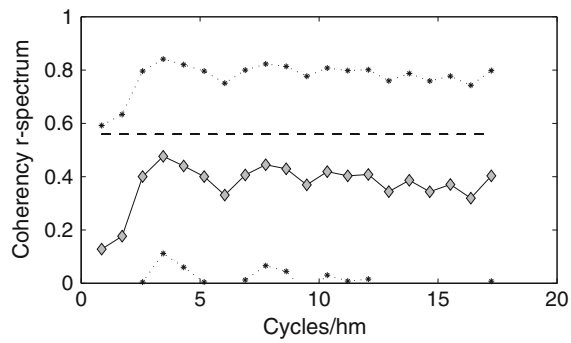

Fig. 8 Cross-spectral comparison between biovolume density and the topographic moisture index (TMI). Coherency r-spectrum. Diamonds: smoothed estimator. Dots: confidence intervals (CI) indicating two standard deviations (95%) on each side of the smoothed estimator. Dashes: confidence threshold indicating the 95% test for difference from null coherency

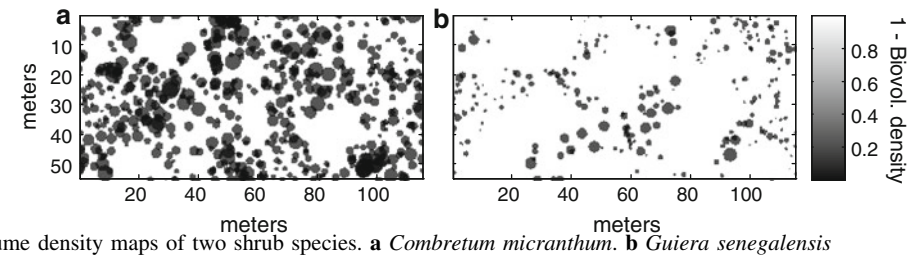

Fig. 9 Biovolume density maps of two shrub species. **a** *Combretum micranthum*. **b** *Guiera senegalensis*

To illustrate a case of scale-specific dependence, we compared the biomass density maps of two dominant shrub species, C*ombretum micranthum* G. Don. and *Guiera senegalensis* J.F. Gmel (Fig. 9).

We observed a significant peak in the coherency values for frequencies characterizing the general vegetation pattern (around 2 cycles/hm) (Fig. 10a). However, the patches dominated by each of the two species appeared spatially distinct, resulting in a phase shift of $\pi/2$ in most directions at the coherent frequencies (Fig. 10b). This scale-specific relationship combined with a phase shift produces, as expected, a very low (ca. 0.1) Pearson's correlation between the two processes. Interestingly, *G. senegalensis* showed a significant coherency with topography (TMI) around the scale of the periodic pattern (result not shown). Phase information indicated that patches of this species were located in the locations of maximum TMI values.

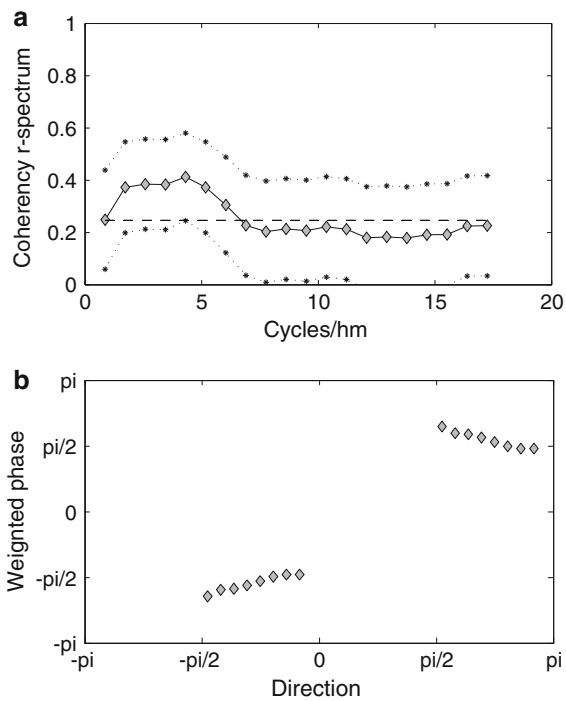

Fig. 10 Cross-spectral analysis between the biomass density maps of *Combretum micranthum* and *Guiera senegalensis*. **a** Coherency r-spectrum. Diamonds: smoothed estimator. Dots: confidence intervals (CI) indicating two standard deviations (95%) on each side of the smoothed estimator. Dashes: confidence interval indicating the 95% test for difference from null coherency. **b** Coherency-weighted average value of the phase for the frequencies and directions in which coherency is maximized

Discussion

In this paper, we illustrated the operational potential of two-dimensional cross-spectral analysis for ecological investigation. We applied the method to a spatially periodic gapped vegetation pattern in SW Niger, and the results refuted the hypothesis that the pattern resulted from particular topographic setups, either directly or via the relief-induced redistribution (run-off) of water resources, as initially hypothesized by Klausmeier (1999). Moreover, previous evidence underscored the need for a scale-specific approach to this question, as vegetation/run-off relationships have been shown to vary non-linearly with scale (Wilcox et al. 2003; Wu 2005). Using cross-spectral analysis, we showed that the independence between vegetation and topography held across the considered range of scales (10–50 m), and therefore also at the scale of the gapped periodic pattern of interest (50 m). The only exception was found for patches of the species *Guiera senegalensis*, which dominated distinct zones within the overall pattern (Diouf et al. in press) and seemed to be favored in locations of relief-induced water concentration. These results have fundamental implications for understanding the nature of self-organization processes in semi-arid patterned landscapes (Barbier et al. 2008). Using a classical (spatially non-explicit) approach would have simply

led to invalid interpretations for the real-world examples we have considered. In contrast, the cross-spectral method was a flexible and efficient approach to test for scale-specific correlations between mapped structures.

If either grid or point-map data are available, cross-spectral techniques are an alternative to more popular techniques based on cross-covariance functions (or on the closely related covariograms; (Wackernagel 1995)). Mathematically, the periodogram and cross-periodogram directly derive from, and are equivalent to, the auto- and cross- covariance functions, and they are in fact the Fourier transform. In practice, however, each approach emphasizes different properties of the structure and covariance structure. The cross-spectrum is a very efficient technique to analyze superimposed structures at different scales and with different levels of anisotropy, and simplified indices are easily derived from it. In contrast, the auto- and cross- covariance functions may be more accurate to quantify monoscale fine-grained structures. The covariogram, which is extensively used in geostatistics, presents limitations with respect to the characterization of shifted (i.e., out of phase) structures (Wackernagel 1995).

One limitation of the analyses detailed in this paper is that they require grid data (either sampled as such or through interpolation) and rectangular study sites, and this differs from approaches based on spatial correlation functions. Yet, "spectral" decomposition on ad-hoc eigenvector maps of the spatial distribution of the sampling points (which have appeared in ecology through the PCNM or MEM methods (Dray et al. 2006)) could help in the future to extend the concept of cross-spectral analyses to irregularly sampled data (MEM eigenvectors are equivalent to the Fourier bases in the case of regular sampling and periodic boundary conditions). An alternative pathway to use cross-spectra to analyze irregularly sampled data is the marked-point process framework (Mugglestone and Renshaw 1996a, b, 2001; Capobianco and Renshaw 1998; Renshaw and Sarkka 2001; Renshaw 2002).

The cross-spectral methods presented in this paper can be used to study anisotropic and/or shifted structures in addition to scale-specific correlations between variables. In studies involving a larger number of variables (signals) (Granger 1964; Priestley 1981), multivariate approaches are also possible that parallel multivariate covariance and cross-covariance functions (Wagner 2004; Couteron and Ollier 2005).

The rapid development of wavelet approaches could lead to improvements in the cross-spectral tools presented in this paper. Indeed, the use of cross-wavelet analysis may be more efficient for some signal structures that are difficult to fit using the sine/cosine functions of the Fourier transform (e.g., step structures). Cross-wavelet analysis can also help with non-stationarity issues, and it may analyse local correlations in a more efficient way than the windowed cross-spectral Fourier approach (Torrence and Compo 1998; Grinsted et al. 2004). However, the huge literature on 2D wavelets is, to date, mainly devoted to image denoising and compression with limited examples of real-world pattern analyses, even in the broader field of earth observation. Its limited use may be due to the difficulty in deriving ecologically meaningful indices from the complex sets of coefficients produced by any type of 2D wavelet transform. Additionally, the statistical properties of Fourier cross-spectral functions are well understood, at least in 1D, which allowed us to use analytically derived significance tests (Appendix). This is not the case for cross-wavelet functions, which still require the use of Monte Carlo simulations for testing correlations under specific assumptions regarding signal structure (Grinsted et al. 2004; Maraun and Kurths 2004).

The Fourier transform is efficiently estimated by the FFT algorithm (including in two dimensions), available in most programming environments (such as R, Matlab, IDL and others). However, contrary to the case of one-dimensional (temporal) analysis, built-in applications to perform 2D cross-spectral analysis are rarely found in statistical packages. Yet, we argue that given the broad use of spectral and cross-spectral approaches and of the Fourier transform in general in other fields of science, their use in ecological studies may increase the communicability of ecological results. At a time of expanding accessibility to spatially explicit data, even for non-scientific audiences via virtual globe interfaces, tools need to be developed that will allow the available information to be utilized, and the resulting advancements to be spread.

Acknowledgements We wish to thank the Ecopas/UE project for scientific and technical support. We are also indebted to Dr. J. Ludwig and Dr. M. Mugglestone, as well as the anonymous reviewers that provided comments on the manuscript.

References

Anderson JM, Mikhail EM (1998) Surveying, theory and practice. WCB/McGraw-Hill, Boston

Barbier N, Couteron P, Lejoly J, Deblauwe V, Lejeune O (2006) Self-organised vegetation patterning as fingerprint of climate and human impact on semiarid ecosystems. J Ecol 94:537–547

Barbier N, Couteron P, Lefever R, Deblauwe V, Lejeune O (2008) Spatial decoupling of facilitation and competition at the origin of gap vegetation patterns in SW Niger. Ecology 89:1521–1531

Bloomfield P (1976) Fourier analysis of time series: an introduction. Wiley, New York

Capobianco R, Renshaw E (1998) The autocovariance function for marked point processes: a comparison between two different approaches. Biometrical J 40:431–446

Chen CH, Pau LF, Wang PSP (1999) Handbook of pattern recognition & computer vision. World Scientific, River Edge, NJ

Couteron P (2001) Using spectral analysis to confront distributions of individual species with an overall periodic pattern in semi-arid vegetation. Plant Ecol 156:229–243

Couteron P (2002) Quantifying change in patterned semi-arid vegetation by Fourier analysis of digitized aerial photographs. Int J Remote Sens 23:3407–3425

Couteron P, Kokou K (1997) Woody vegetation spatial patterns in a semi-arid savanna of Burkina Faso, West Africa. Plant Ecol 132:211–227

Couteron P, Ollier S (2005) A generalized, variogram-based framework for multi-scale ordination. Ecology 86:828–834

Couteron P, Pelissier R, Nicolini EA, Paget D (2005) Predicting tropical forest stand structure parameters from Fourier transform of very high-resolution remotely sensed canopy images. J Appl Ecol 42:1121–1128

Couteron P, Barbier N, Gautier D (2006) Textural ordination based on Fourier spectral decomposition: a method to analyze and compare landscape patterns. Landscape Ecol 21:555–567

Cressie NAC (1993) Statistics for spatial data. Wiley, New York

Diggle P (1989) Time series: a biostatistical introduction. Oxford University Press, Oxford

Diouf A, Barbier N, Mahamane A, Lejoly J, Saadou M, Bogaert J (in press) Analyse de la structure spatiale des individus ligneux dans «une brousse tachetée» au Sud Ouest du Niger. Can J Forest Res

Dray S, Legendre P, Peres-Neto PR (2006) Spatial modelling: a comprehensive framework for principal coordinate analysis of neighbour matrices (PCNM). Ecol Model 196:483–493

Fisher NI (1993) Statistical analysis of circular data. Cambridge University Press, Cambridge

Ford ED (1976) The canopy of Scots pine forest: description of a surface of complex roughness. Agr Forest Meteorol 17:9–32

Forman RTT, Godron M (1986) Landscape ecology. Wiley, New York

Fuentes M (2002) Spectral methods for nonstationary spatial processes. Biometrika 89:197–210

Granger CWJ (1964) Spectral analysis of economic time series. Princeton University Press, Princeton

Grinsted A, Moore JC, Jevrejeva S (2004) Application of the cross wavelet transform and wavelet coherence to geophysical time series. Nonlinear Proc Geoph 11:561–566

HilleRisLambers R, Rietkerk M, van den Bosch F, Prins HHT, de Kroon H (2001) Vegetation pattern formation in semi-arid grazing systems. Ecology 82:50–61

Hutchinson J, Dalziel JM, Keay RWJ, Hutchinson J (1954) Flora of west tropical Africa. Published under the authority of the Secretary of State for the Colonies by the Crown Agents for Oversea Governments and Administrations, London

Jenkins GM, Watts DG (1968) Spectral analysis and its applications. Holden-Day, San Francisco

Keitt TH (2000) Spectral representation of neutral landscapes. Landscape Ecol 15:479–493

Klausmeier CA (1999) Regular and irregular patterns in semiarid vegetation. Science 284:1826–1828

Lefever R, Lejeune O (1997) On the origin of tiger bush. B Math Biol 59:263–294

Legendre P (1993) Spatial autocorrelation—trouble or new paradigm. Ecology 74:1659–1673

Levin SA (1992) The problem of pattern and scale in ecology. Ecology 73:1943–1967

Maraun D, Kurths J (2004) Cross wavelet analysis: significance testing and pitfalls. Nonlinear Proc Geoph 11:505–514

McIntire EJB, Fajardo A (2009) Beyond description: the active and effective way to infer processes from spatial patterns. Ecology 90:46–56

Mugglestone MA, Renshaw E (1996a) The exploratory analysis of bivariate spatial point patterns using cross-spectra. Environmetrics 7:361–377

Mugglestone MA, Renshaw E (1996b) A practical guide to the spectral analysis of spatial point processes. Comput Stat Data Anal 21:43–65

Mugglestone MA, Renshaw E (1998) Detection of geological lineations on aerial photographs using two-dimensional spectral analysis. Comput Geosci 24:771–784

Mugglestone MA, Renshaw E (2001) Spectral tests of randomness for spatial point patterns. Environ Ecol Stat 8:237–251

Pascual M, Guichard F (2005) Criticality and disturbance in spatial ecological systems. Trends Ecol Evol 20:88–95

Platt T, Denman KL (1975) Spectral analysis in ecology. Annu Rev Ecol Syst 6:189–210

Priestley MB (1981) Spectral analysis and time series. Academic Press, London

Proisy C, Couteron P, Fromard F (2007) Predicting and mapping mangrove biomass from canopy grain analysis using Fourier-based textural ordination of IKONOS images. Remote Sens Environ 109:379–392

Puech C (1994) Thresholds of homogeneity in targets in the landscape—relationship with remote-sensing. Int J Remote Sens 15:2421–2435

Quinn PF, Beven KJ, Lamb R (1995) The ln(a/tan-beta) index—how to calculate it and how to use it within the Topmodel framework. Hydrol Process 9:161–182

Rayner JN (1971) Introduction to spectral analysis. Pion Ltd., London

Renshaw E (2002) Two-dimensional spectral analysis for marked point processes. Biometrical J 44:718–745

Renshaw E, Ford ED (1983) The interpretation of process from pattern using two-dimentional spectral analysis: methods and problems of interpretation. Appl Stat 32:51–63

Renshaw E, Ford ED (1984) The description of spatial pattern using two-dimensional spectral analysis. Vegetatio 56: 75–85

Renshaw E, Sarkka A (2001) Gibbs point processes for studying the development of spatial-temporal stochastic processes. Comput Stat Data Anal 36:85–105

Rietkerk M, van de Koppel J (2008) Regular pattern formation in real ecosystems. Trends Ecol Evol 23:169–175

Ripley BD (1981) Spatial statistics. Wiley, New York

Rohani P, Lewis TJ, Grunbaum D, Ruxton GD (1997) Spatial self-organization in ecology: pretty patterns or robust reality? Trends Ecol Evol 12:70–74

Schneider DC (2001) The rise of the concept of scale in ecology. Bioscience 51:545–553

Solé RV, Bascompte J (2006) Self-organization in complex ecosystems. Princeton University Press, Princeton

Sorensen R, Zinko U, Seibert J (2005) On the calculation of the topographic wetness index: evaluation of different methods based on field observations. Hydrol Earth Syst Sci Discuss 2:1807–1834

Tang XO, Stewart WK (2000) Optical and sonar image classification: Wavelet packet transform vs Fourier transform. Comput Vis Image Und 79:25–46

Torrence C, Compo GP (1998) A practical guide to wavelet analysis. Bull Am Meteorol Soc 79:61–78

von Hardenberg J, Meron E, Shachak M, Zarmi Y (2001) Diversity of vegetation patterns and desertification. Phys Rev Lett 8719

Wackernagel H (1995) Multivariate geostatistics: an introduction with applications. Springer, Berlin

Wagner HH (2004) Direct multi-scale ordination with canonical correspondence analysis. Ecology 85:342–351

Wiens JA (1989) Spatial scaling in ecology. Funct Ecol 3: 385–397

Wilcox BP, Breshears DD, Allen CD (2003) Ecohydrology of a resource-conserving semiarid woodland: effects of scale and disturbance. Ecol Monogr 73:223–239

Wu XB (2005) Scale-dependent influence of topography-based hydrologic features on patterns of woody plant encroachment in savanna landscapes. Landscape Ecol 20: 733–742